Effects of co-exposure to benzo-a-pyrene and cerium dioxide nanoparticles on human lung and placental barriers

Gaëlle Deval, Safaa Mawas, Stéphanie Devineau, Didier Borderie, Claire Mikolajczak, Grégory Lefèvre, Linh-Chi Bui, Justine Renault, Charlotte Izabelle, Thierry Fournier, et al.

Journal of Hazardous Materials Advances 19 (2025) 100802

Contents lists available at ScienceDirect

Journal of Hazardous Materials Advances

journal homepage: www.elsevier.com/locate/hazadv

Effects of co-exposure to benzo-a-pyrene and cerium dioxide nanoparticles on human lung and placental barriers

Gaëlle Deval [a], Safaa Mawas [b], Stéphanie Devineau [b], Didier Borderie [c], Claire Mikolajczak [a], Grégory Lefèvre [d], Linh-Chi Bui [b], Justine Renault [b], Charlotte Izabelle [e], Thierry Fournier [a], Ioana Ferecatu [a,1], Sonja Boland [b,1,*]

[a] Université Paris Cité, INSERM U1139 (FPRM), Faculté de Pharmacie, FHU Prem'Impact, F-75006 Paris, France
[b] Université Paris Cité, CNRS, Unité de Biologie Fonctionnelle et Adaptative, F-75013 Paris, France
[c] AP-HP Centre-Université Paris Cité, Service de Diagnostic Biologique Automatisé, Hôpital Cochin, F-75006 Paris, France
[d] Université PSL, Chimie ParisTech, CNRS IRCP, F-75005 Paris, France
[e] Université Paris Cité, UAR3612 CNRS, US25 Inserm, Plateforme d'Imagerie Cellulaire et Moléculaire PICMO, Faculté de Pharmacie, F-75006 Paris, France

ARTICLE INFO

Keywords:
Cerium dioxide nanoparticles
Nanoceria
Benzo-a-pyrene
AhR
Coating
Human bronchial epithelial cells
Human trophoblasts

ABSTRACT

Cerium dioxide nanoparticles (CeO_2 NPs) are emerging pollutants widely used for their catalytic properties in diesel fuel and cigarettes. Human exposure to CeO_2 NPs rarely occurs in isolation. Benzo-a-pyrene (BaP), a polycyclic aromatic hydrocarbon co-emitted from diesel engines, tends to adsorb onto CeO_2 NPs in contaminated environments. To better understand their combined effects on both the lung and placental tissues which are critical-barriers for the fetus, we coated CeO_2 NPs with BaP at two different ratios, mimicking environmental exposure. We characterized the physicochemical properties of BaP-coated NPs in bronchial and placental culture media, assessed coating stability and BaP desorption. We evaluated the biological impact of BaP-coated CeO_2 NPs on primary normal human bronchial epithelial cells and purified villous cytotrophoblasts from term human placentas. We compared the response of BaP-coated NPs with that observed under parallel co-exposure, and to individual exposures to BaP and CeO_2 NPs. Bronchial cells exhibited toxicity at lower doses under co-exposure by parallel addition compared to BaP-coated NPs. Cytochrome P450 (CYP1A1) induction varied between tissue barriers, exhibiting a BaP dose-dependent response in both tissue models but coating-independent response in trophoblasts, whereas bronchial cells showed a stronger response to BaP adsorbed on CeO_2 NPs. These findings highlight how BaP, when stably associated with CeO_2 NPs, exerts modulated effects depending on the tissue, potentially altering its metabolic kinetics and thus its biopersistence. This study underscores the importance of considering particle-bound pollutants when evaluating the health impact of airborne particulate matter, as this more accurately reflects environmental exposure.

1. Background

Ultrafine particles (UFPs) (particulate matter below 0.1 μm or $PM_{0.1}$) have long been present in the atmosphere as a result of natural combustion processes like wildfires and volcanic activity. However, human activities, particularly those involving the production and use of engineered nanomaterials, such as in electronic devices, automobiles, construction industry, cosmetics, nanomedicine, food, water purification or textiles, have introduced new sources of UFPs (Stone et al., 2017). In addition, in urban environments, CeO_2 NP used in diesel fuel additives are known to be emitted and dispersed as PM, contributing to the atmospheric pollution. Cerium dioxide nanoparticles (CeO_2 NPs) are used as diesel fuel additives to catalyze the combustion of soot for diesel particulate filter regeneration, liberating airborne cerium-based UFPs

* Corresponding author.
E-mail addresses: gaelle.deval@gmail.fr (G. Deval), safaa.mawas@etu.u-paris.fr (S. Mawas), stephanie.devineau@u-paris.fr (S. Devineau), didier.borderie@aphp.fr (D. Borderie), clairemiko7@gmail.com (C. Mikolajczak), gregory.lefevre@chimieparistech.psl.eu (G. Lefèvre), linh-chi.bui@u-paris.fr (L.-C. Bui), justine.renault@u-paris.fr (J. Renault), charlotte.izabelle@u-paris.fr (C. Izabelle), thierry.fournier@u-paris.fr (T. Fournier), ioana.ferecatu@u-paris.fr (I. Ferecatu), sonja.boland@u-paris.fr (S. Boland).
[1] Equal contributions

https://doi.org/10.1016/j.hazadv.2025.100802
Received 27 February 2025; Received in revised form 13 June 2025; Accepted 26 June 2025
Available online 27 June 2025

(Gantt et al., 2014). These emitted particles can be coated with organic molecules produced by the combustion process that may influence their toxicity, highlighting the need for specific toxicological evaluations of combustion-derived NPs. Numerous epidemiological studies have demonstrated a correlation between high exposure to UFPs and chronic respiratory pathologies (Leikauf et al., 2020) and pregnancy complications (Johnson et al., 2021). Indeed, the lungs and placenta are barrier organs that protect the fetus from certain xenobiotics in air pollution that the mother is exposed to during pregnancy. However, these barrier functions are not entirely effective against UFPs, as some can bypass them to reach systemic and fetal circulation, potentially altering the functioning of these key organs (Bongaerts et al., 2020).

In the early 2000s, CeO_2 NPs, also named nanoceria, began to be used for their catalytic properties as additives in diesel fuel (Wakefield et al., 2008) and cigarettes (Böhlandt et al., 2012). Their anti- and/or pro-oxidant properties also make them interesting for the treatment of various diseases, such as cancers (Kargozar et al., 2018; Casals et al., 2020; Saifi et al., 2021). Their ability to absorb UV makes them a potential alternative to titanium dioxide NPs used in sunscreens (Miri et al., 2020). Given their broad range of applications, environmental and occupational exposure to CeO_2 NP is expected to increase. To date, the major exposure route to CeO_2 NPs is inhalation. Their ultrafine size, low density (1.5–2.4 g/cm^3) and high stability in air facilitate their airborne persistence and penetration into the respiratory tract, including the alveolar region (Park et al., 2008; Gantt et al., 2014; Paul et al., 2017; Guo et al., 2019; Gosens et al., 2024; Li et al., 2025). For example, their use as diesel additives has increased the cerium content in exhaust gases from 0.3 % to 6.5 % (Zhang et al., 2016) accompanied by an increase in benzo(a)pyrene (BaP) emissions by 35 % (Zhang et al., 2013). Moreover, their nanoscale size gives them a high surface area, promoting their coating with organic molecules, including pollutants emitted during combustion processes, such as polycyclic aromatic hydrocarbons (PAH). The composition of this organic coating around CeO_2 NPs can lead to changes in their physicochemical properties (Yokel et al., 2019), the internalization of these NPs by cells, the bioavailability and metabolization of the adsorbed organic molecules, and consequently, to the toxicity of both the organic and inorganic pollutants (Mazzolini et al., 2016).

In 2010, the OECD called for an urgent evaluation of CeO_2 NPs to assess their impact on human health. Consequently, several studies have been conducted, using animal models and human cell lines. However, very few studies have considered their interaction with other pollutants such as BaP (Zhang and Balasubramanian, 2017; Cotena et al., 2021; Deval et al., 2023) and for our knowledge no study has used coated CeO_2 NPs.

BaP is recognized as the prototype PAH, classified as certain carcinogen, mutagen, and reproductive toxicant (CMR) by the International Agency for Research on Cancer (IARC, 2010), as well as an endocrine disruptor (Zhao et al., 2014; Sheweita et al., 2016; Guarnieri et al., 2023). Highly lipophilic BaP can easily cross the plasma membrane to be internalized into cells. Its ability to bypass pulmonary and placental barriers has already been demonstrated (Arnould et al., 1997). Once BaP penetrates the cells, it will be metabolized through the detoxification pathway involving the aryl hydrocarbon receptor (AhR), leading to the production of mutagenic metabolites that cause DNA damage and can also induce excessive production of reactive oxygen species (ROS), resulting in oxidative stress. Respiratory exposure to BaP has been associated with the development of chronic lung diseases and cancers (Li et al., 2024). Epidemiological studies have correlated BaP exposure during pregnancy with an increased risk of spontaneous miscarriages (Dai et al., 2023), low birth weights (Duarte-Salles et al., 2013), and preterm births (Suter et al., 2019). In human trophoblastic cell lines, exposure to BaP can be cytotoxic, cause cell cycle arrest, and lead to cell migration and invasion inability (Le Vee et al., 2014; Wang et al., 2017). BaP-coated CeO_2 NPs raise important questions about the potential toxicity of BaP after adsorption onto CeO_2 NPs. In a Trojan horse hypothesis, the exposure to BaP-coated CeO_2 NPs may increase or alternatively decrease BaP bioavailability following NP internalization. Additionally, this coating could influence the metabolization of BaP by AhR pathway-mediated detoxification enzymes, potentially altering the cellular response to this environmental pollutant.

The bronchial epithelium is the first cellular barrier in contact with airborne pollutants. It is composed of various cell types, including ciliated epithelial cells, goblet cells, and basal cells, which together play a critical role in protecting the respiratory system from pollutants and pathogens. Normal human bronchial epithelial (NHBE) cells are derived from biopsies of bronchial epithelium and are commonly used in primary culture models to study the respiratory epithelium. In culture, NHBE cells can maintain their differentiated state and form a pseudostratified epithelium that includes goblet cells, which secrete mucus; and basal cells, which serve as progenitor cells for the epithelium. The xenobiotic metabolizing activity of the epithelium is also maintained when culturing NHBE cells, making primary NHBE culture model a valuable tool for investigating cellular responses to environmental pollutants due to its ability to closely mimic the *in vivo* conditions of the human bronchial epithelium.

The placenta, a temporary organ essential for the course of pregnancy, has chorionic villi as its structural and functional unit, anchored in the maternal endometrium. These villi are composed of a mesenchymal core containing fetal vessels, surrounded by an underlying layer of villous cytotrophoblasts (VCT). Throughout pregnancy, VCT differentiate by fusing with the outermost layer, the syncytiotrophoblast (ST), which plays a major role in the endocrine function of the placenta. This outer layer is in direct contact with maternal blood present in the intervillous space and thus potentially with pollutants. Access to the placenta after delivery allows for the isolation of VCT to establish primary cultures. One of the advantages of the primary VCT culture model is their spontaneous differentiation into ST with an endocrine activity (Kliman et al., 1986), which makes it a relevant study model of the impact of pollutants on the placental barrier (Deval et al., 2021). Furthermore, in primary VCT culture model, AhR has a constitutive nuclear localization in VCT and ST. Moreover, differentiation into ST leads to a significant upregulation of AhR target genes CYP1A1 and CYP1B1, suggesting AhR activation during trophoblast differentiation as a physiological function (Wakx et al., 2018).

We previously studied the impact of co-exposure to CeO_2 NPs with BaP on a primary human trophoblast culture model by parallel addition (Deval et al., 2023). This co-exposure induced cellular stress mediated by activation of the AhR pathway, leading to elevated p53 and p21 protein levels. BaP-induced DNA damage was reduced during co-exposure with CeO_2 NPs. However, a limitation of this study was that the two pollutants (BaP and CeO_2 NPs) were introduced simultaneously as free compounds in the culture, whereas in real environmental conditions, such as those encountered in diesel exhaust, NPs and PAHs will interact prior to inhalation as they have a high affinity for particulate matter. These interactions would lead to the formation of hybrid airborne particles where BaP is adsorbed onto the surface of CeO_2 NPs and may alter the physicochemical properties, bioavailability, cellular uptake, and toxicity of both the NP and the adsorbed PAH compound. Therefore, our aim was not only to assess toxic effects, but also to determine whether the mode of co-exposure (free versus adsorbed BaP) plays a role in the modulation of the biological response at both the pulmonary and the placental barrier (the two major barriers for the foetus). We believe this exposure strategy offers more environmentally relevant insights than either compound alone or by parallel addition *in vitro*. Thus, to better approximate these environmentally relevant exposure scenarios and assess whether this interaction alters biological effects, we coated CeO_2 NPs with BaP to study their impact on the pulmonary and placental barriers. We performed this coating at two controlled BaP/CeO_2 NPs ratios:

- A low ratio of 1.66 mg (BaP)/g (CeO_2 NPs) approximating that of UFP/PAH found in Parisian atmospheric pollution (Val et al., 2011), called low-ratio coating (coating LR);
- A higher ratio of 6.64 mg (BaP)/g (CeO_2 NPs), four times higher than the low ratio.

The main objective of this study was to determine whether the mode of co-exposure, either as a parallel exposure to free CeO_2 NPs and BaP or as BaP-coated CeO_2 NPs, could lead to synergistic or counterbalancing effects on toxicity and cellular responses compared to individual exposures. To this end, we first developed a protocol for the coating of CeO_2 NPs with BaP and analyzed the amount of adsorbed BaP using HPLC. The stability of the coating in the culture medium was confirmed by ATR-FTIR spectroscopy. We physically and chemically characterized these BaP-coated CeO_2 NPs in both bronchial and placental culture media and assessed the effective concentration deposited on cells. Subsequently, we studied the cytotoxicity on primary cultures of primary human bronchial epithelial cells (NHBE) and VCT isolated from human term placentas. The ratios used for the parallel co-exposure of the two pollutants were identical to those of the BaP-coated CeO_2 NPs at both high and low ratios to allow for a comparison between the two types of exposure. Finally, we assessed the effects of the different treatments toward AhR detoxification pathway using non-cytotoxic concentrations of the pollutants to assess whether the coating of BaP around CeO_2 NPs can lead to changes in the bioavailability of the adsorbed organic molecules, either increasing its effects through synergistic mechanisms or reducing them by sequestering BaP.

2. Materials and methods

2.1. Coating of CeO_2 NPs with benzo-a-pyrene and preparation of suspensions

CeO_2 NPs were obtained from the Joint Research Centre of the European Union (NM-212, IHCP, Ispra, Italy). According to the repository report JRC89825, these particles are polyhedral with regular morphology, exhibit a non-homogeneous size distribution, ranging from 10 nm to over 100 nm, are uncoated and contain no capping agents. Two ratios of CeO_2 NPs coated with BaP were made for the treatments:

- A first ratio called the “Coating Low Ratio (LR)” approximating the PAH/PUF ratio found in Parisian atmospheric pollution (Val et al., 2011) (0.15 to 2 mg PAH/g PUF converted to 1.66 mg BaP/g CeO_2 NPs, corresponding to 2 μM BaP per 80 μg of CeO_2 NPs/cm^2 of culture if all BaP is desorbed);
- A second ratio, called the "Coating High Ratio (HR)," equivalent to 6.64 mg BaP/ g CeO_2 NPs, corresponding to 8 μM BaP per 80 μg of CeO_2 NPs/cm^2 of culture. This ratio is four times higher than the Low Ratio, simulating a higher exposure scenario while remaining below the amount needed to form a complete monolayer of BaP around the NPs (which would be of 14.5 mg (BaP) /g (CeO_2 NPs)).

The weighed powdered CeO_2 NPs were suspended in glass tubes with cyclohexane (CHX) containing the desired quantity of BaP (Sigma-Aldrich #31,306) depending on whether the HR or LR coating was achieved. After homogenization by stirring on vortex at high intensity for one minute, the CeO_2 NPs solutions were distributed homogeneously into 2 mL glass tubes so that each tube contained 3 mg of CeO_2 NPs. The solutions were kept under a fume cupboard for 24 h to allow the CHX to completely evaporate. The tubes were then sealed with sterilized plastic caps. Control CeO_2 NPs were suspended in CHX (Sigma-Aldrich #227,048) without BaP (referred to as CHX-treated CeO_2 NPs) and CHX was subsequently evaporated.

CHX-treated CeO_2 NPs, and BaP-coated CeO_2 NPs at low and high ratios were diluted in bronchial or placental culture medium supplemented with 10 % fetal calf serum (FCS, Eurobio #CVFSVF00–01, Les Ulis, France) at a concentration of 3 mg/mL and sonicated with a cup horn (450 W and 50/60 Hz, Branson, Danbury, CT, USA) at 70 % amplitude, on ice, for 2 min.

2.2. Dynamic light scattering

Size distribution of CeO_2 NPs was measured by dynamic light scattering (DLS) at 37 °C with a Zetasizer Nano-ZS (Malvern Instruments, Ltd, Worcestershire, UK). DLS measurements were conducted with particle suspensions in triplicate with a particle concentration of 0.03 mg/mL in milliQ H_2O at 37 °C and a scattering angle of 173°. Measurements were fitted using the Smoluchowski model. The first DLS measurement was done at $t = 0$ after sonication. The suspension was then placed in a 48-well culture plate in an incubator at 37 °C, 5 % CO_2 corresponding to treatment conditions. DLS measurements were performed after 24 h and 48 h incubation.

2.3. Effective density determination and dosimetry modeling

The effective density was established by the Volumetric Centrifugation Method (VCM) and the deposited fraction of CeO_2 NPs was calculated on DosiGUI by the one-dimensional Distorted Grid (DG) model developed by DeLoid et al. (DeLoid et al., 2015). CeO_2 NPs treated with CHX and coated with BaP at both ratios were suspended at 1 mg/mL in bronchial and placental media ($n = 2$ for each condition). The suspensions were centrifuged at 3000 g in PCV tubes (TPP #87,005 Switzerland) for 1 hour. To obtain the volume of the CeO_2 NPs pellets collected at bottom of the capillary in each tube, the ‘easy-read’ measuring device (TPP #87,010 Switzerland) was used. The effective density was calculated using the following formula:

$$\rho_{EV} = \rho_{\text{media}} + \left[\left(\frac{m_{\text{ENM}} - m_{\text{ENMsol}}}{V_{\text{pellet}} \cdot SF}\right)\left(1 - \frac{\rho_{\text{media}}}{\rho_{\text{ENM}}}\right)\right]$$

where:

ρ_{EV} is the effective volumetric density of CeO_2 NPs, ρ_{media} the density of the medium, m_{ENM} the mass of the CeO_2 NPs, m_{ENMsol} the mass of CeO_2 NPs suspended, V_{pellet} the volume of the CeO_2 NPs pellet, *SF* the structure factor (0.634 for irregularly packed spheres), and ρ_{ENM} the intrinsic density of the CeO_2.

2.4. Attenuated total reflectance fourier-transform infrared (ATR-FTIR)

ATR-FTIR spectra were measured with a Thermo Scientific Nicolet 6700 FTIR spectrometer equipped with a mercury cadmium telluride detector cooled at 77 K by liquid nitrogen. The ATR accessory was a horizontal ZnSe crystal coated with diamond ($A = 2.54\ mm^2$) with single reflection and an angle of incidence of 45° (Smart Miracle from PIKE). Spectral resolution was 4 cm^{-1}. 256 scans were averaged and OMNIC software was used for the data collection and treatment.

2.5. BaP quantification with reverse phase-hight pressure liquid chromatography (RP-HPLC)

Quantification of adsorbed BaP: BaP was desorbed from CeO_2 NPs by adding 1 mL of LC-MS grade acetonitrile (12,078, Biosolve) to 1.5 mg of LR or HR BaP-coated CeO_2 NPs in glass tubes. The suspension was incubated on a wheel at room temperature overnight. The solution was then transferred to an Eppendorf tube and centrifuged for 30 min at 15,000 g at 4 °C to pellet CeO_2 NPs. The supernatant was then collected and filtered with a 0.2 μm polytetrafluoroethylene syringe filter (#15,141,499, Thermo Fisher Scientific). The filtered solution was then diluted (1:1000 for HR coating and 1:100 for LR coating) in acetonitrile (ACN). 1 μL was injected on the HPLC system. The amount of adsorbed BaP expressed as a mass ratio (g(BaP)/g(CeO_2 NPs) was calculated as follows:

$$R(g\ BaP\ /\ g\ CeO2\ NPs) = \frac{[BaP]\ x\ V}{m\ (CeO2)}$$

where [BaP] is the concentration of measured BaP in g/L, V (L) is the solvent volume and m(CeO_2) (g) the mass of CeO_2 NPs.

Quantification of BaP desorbed after sonication of BaP-coated CeO_2 NPs in cell culture media: the BaP-coated CeO_2 NPs were resuspended in placental or bronchial culture media and sonicated as described in the treatment protocol. The suspension was then centrifuged for 30 min at 15,000 g at 4 °C to pellet CeO_2 NPs. The supernatant was collected and diluted 10 times in acetonitrile for BaP extraction. 2 µL were injected on the RP-HPLC system.

Reverse Phase HPLC analysis was performed on a Kinetex F5 column (OOD-4723-EO, 100 × 4.6 mm, 2.6 µm, Phenomenex) at a constant flow rate of 1 $L.min^{-1}$ at 30 °C for 12 min. The mobile phase composition was LC-MS grade water for mobile phase A and 100 % LC-MS grade acetonitrile for mobile phase B. The gradient steps were 30 % A + 70 % to 100 % B from 0 to 10 min and 30 % A + 70 % B from 10 to 12 min. BaP was detected by fluorescence (excitation at 365 nm, emission at 405 nm) and quantified with LabSolution software by integration of the peak area.

2.6. Normal human bronchial epithelial (NHBE) culture

Primary NHBE cells were purchased from Lonza (CC-2540S) and used from passage 1 till 8. NHBE cells were cultured in PneumoCult-Ex plus basal medium (StemCell 05,041), supplemented with PneumaCult™-Ex Plus 50X Supplement (StemCell 05042). Cells were cultured at a density of 5000 cells/cm^2 in 25 cm^2 or 75 cm^2 culture flasks (Corning) at 37 °C in a humidified 5 % CO_2 atmosphere. Once reached 70–80 % confluence, cells were dissociated using the animal Component-Free Cell Dissociation kit (StemCell 05426). For exposure, cells were seeded at a density of 50,000 cells/cm^2 in 6 well-plates for western blot (Costar, Corning) and 48 well-pates for WST-1 and AlamarBlue assay (Corning). Culture medium was changed every 2 days with 0.25 mL for the 48 well-plates and 2 mL for 6 well-plates.

2.7. Placenta collection

The study was performed according to the principles of the Declaration of Helsinki. Placentas were collected from nonsmoking women with physiological pregnancies delivered by caesarean section between 39 and 41 weeks of amenorrhea. Placentas were obtained with approval from our local ethics committee (CPP: 2015-May-13,909) and after obtaining written consent from informed patients, from maternity hospitals in the Île- de-France region: the Institut Mutualiste Montsouris, the Private Hospital of Antony and the Diaconesses Hospital.

2.8. Cytotrophoblast purification and culture

The isolation and primary culture of trophoblasts was carried out according to the protocol used previously (Deval et al., 2023). After collection, placental tissues were washed in Ca^{2+} and Mg^{2+} free Hank's balanced salt solution (HBSS, Gibco #14175, Thermo Fisher Scientific, Illkirch, France). Chorionic villi were scraped from vessels and connective tissue and dissected to recover approximately 20 mg of tissue. The time for placental dissection was kept under 30 min to prevent tissue degradation. The mononucleated villous cytotrophoblasts were isolated, based on the methods of Kliman et al. (Kliman et al., 1986). After dissection, the chorionic villi were washed in $Ca^{2+}$and Mg^{2+} free HBSS, and then digested in trypsin digestion medium containing HBSS 5 mL/g, 0.1 % trypsin (Gibco #27250–018), 0.1 M $MgSO_4$ (Merck #5886–0500, New York, NY, USA), 0.1 M $CaCl_2$ (Merck #1–02820–1000), 4 % non-fat milk (Biocoop), and 50 Kunitz/mL DNAse type IV (Sigma-Aldrich #D5025, Saint Quentin Fallavier, France), for 30 min at 37 °C without stirring. The following digestions of 10 min, with renewal of the trypsin solution at each digestion, were monitored by observation under an optical microscope. Digestions containing a majority of VCT were kept and pooled. The chorionic villi were finally washed with warm HBSS (37 °C). Each time, the supernatant containing VCT was collected after tissue sedimentation, filtered on 40 µm pore filters, and incubated with 10 % fetal calf serum (FCS, Dutscher, #S1900–500C) to stop the trypsin activity. After purification by Percoll (GE Healthcare # 17–5445–01) gradient, VCT were resuspended and cultured in Dulbecco's modified Eaglets medium (DMEM, containing 1 g/L glucose, pyruvate, without phenol red, Thermo Fisher Scientific, #11,880, Illkirch, France) supplemented with 10 % FCS (Eurobio #CVFSVF00–01, Les Ulis, France), 2 mM glutamine (Sigma-Aldrich #G7513), 100 IU/mL penicillin, and 100 µg/mL streptomycin (Gibco #15140–122, Thermo Fisher Scientific) at 150,000 cells/cm^2 on 48 well-plates for WST-1 and 60 mm diameter culture dishes for western blot. After around 16 h of culture, VCT were carefully washed to eliminate nonadherent cells.

2.9. Bronchial epithelial cell and cytotrophoblast treatments

Trophoblasts were cultured overnight while primary bronchial epithelial cells for 48 h, then washed with fresh media before incubation with 250 µL/48-well plate, 2.5 mL/6 well plates and 5 mL for 60 mm dishes of BaP and/or CeO_2 NPs for 24 and 48 h at different concentrations (1.25 to 80 µg/cm^2 for CeO_2 NPs and 0.03 to 8 µM for BaP). CeO_2 NPs were dispersed in DMEM cell culture media without FCS for VCT and in PneumoCult-Ex Plus for NHBE cells at a concentration of 3 mg/mL and sonicated on ice for 2 min as described before. CeO_2 NPs were then sequentially diluted in respective cell culture medium immediately before use. Staurosporin (STS, Sigma-Aldrich #S4400) was used at a final concentration of 0.5 µM for 3 h for trophblasts and 1.5 µM for 48 h in NHBE cells and ter-Butyl hydroperoxide (tBHP, Luperox TBH70X solution, Sigma-Aldrich #458139) at 500 µM for 48 h.

2.10. Metabolic activity by WST-1

Metabolic activity was assessed using the WST-1 assay (Sigma-Aldrich #11644807001) according to the manufacturer's instructions. At the end of the exposure time, cells were rinsed with culture medium and then WST-1 reagent was added (150 µL/well at 1:100 in culture medium for trophoblasts and 200 µL/well at 1:30 in MEM culture media (Gibco #51200, ThermoFisher) for NHBE) to each well and incubated for 3 h for trophoblasts and 0.5 to 1 h for NHBE cells at 37 °C. Absorbance at 440–450 nm was measured using a microplate reader (EnSpire 2300 Multilabel reader, PerkinElmer, Villebon-sur-Yvette, France or BioTek EL808, Fisher Scientific, Illkirch, France) and subtracted from the baseline measured at 570–600 nm. To test for potential interference of CeO_2 NPs with WST-1 assay, the same experiment was performed followed by the addition of Triton at 0.1 % (Sigma-Aldrich, Triton X100–100 mL) to each well 15 min before adding WST-1 reagent. The corresponding absorbances were subtracted from the results to eliminate interferences from CeO_2 NPs.

2.11. LDH assay

At the end of treatment time, the media was collected and stored at −20 °C until analysis. For NHBE cells, extracellular LDH was quantified by CytoTox 96® Non-Radioactive Cytotoxicity Assay (Promega #G1780) according to the supplier's instructions and absorbencies measured at 490 nm using a microplate reader (BioTek EL808). For VCT, extracellular LDH assay was performed using a Cobas c 701 analyzer (Roche Diagnostics) with UV test methodology. The linear range for LDH activity measurement was between 10–1000 UI/L (0.17–16.7 µkat/L). The lower limit of detection for the assay was 2 UI/L. For VCT, the LDH assay results were normalized to the amount of total protein quantified using the Pierce™ BCA Protein Assay Kit (Thermo Fisher Scientific #23235) to account for VCT loss during and after the purification

protocol.

CeO_2 NPs interference test with LDH assay: Bare and coated CeO_2 NPs at LR and HR at a concentration of 80 μg/cm^2 were incubated for 48 h with 1 μL of LDH positive control from the CytoTox 96® Non-Radioactive Cytotoxicity Assay (purified Lactate Dehydrogenase from rabbit muscle) in placental and bronchial culture medium. The placental culture medium containing LDH was used as a control to represent 100 % of the LDH amount added during incubation. The supernatants were centrifuged for 3 min at 500 g to remove the NPs. LDH measurement was performed using a Cobas c 701 analyzer for the placental medium and with CytoTox 96® Non-Radioactive Cytotoxicity Assay for the bronchial medium

2.12. Alamar blue

At the end of treatment time, cultures were rinsed with culture media and AlamarBlue™ (AB, Thermo Fisher Scientific #DAL1100) was diluted (1:10 ratio) in HBSS containing Ca^{2+}/Mg^{2+} (Gibco #14025-092 ThermoFisher) and 200 μL was added to control and treated cultures. After 0.5–1 h incubation at 37 °C, 100 μL of the medium were transferred to a 96-well clear bottom microplate (μClear®, Greiner Bio-One, Dominique Dutscher, Bernolsheim France). The fluorescence was measured on FlexStation 3 multi-mode microplate reader (Molecular Devices, San Jose, California) with excitation and emission wavelengths set at 545 nm and 590 nm respectively.

2.13. Protein extraction and western blot

Total protein extracts from trophoblast cells from 60 mm dish cultures or NHBE cells from 6-well culture dishes were obtained after washing cultures with cold Ca^{2+} and Mg^{2+} free HBSS by harvesting cells by adding 53 μL/well for NHBE and 70 μL/dish for trophoblasts of Ripa lysis buffer (Cell Signaling #9806S), with added protease inhibitors (1:100, Protease Inhibitor Cocktail Set I, Calbiochem Merck #539131) and phosphatase inhibitors (1:50, Phosphatase Inhibitor Cocktail Set V, Calbiochem Merck #524629). Protein extracts were centrifuged for 5 min at 14,000 g and stored at −80 °C. Protein concentrations were determined using the Pierce™ BCA Protein Assay Kit (Thermo Fisher Scientific #23235). Equal amounts of proteins (30 μg) were separated on 4–15 % SDS-PAGE mini-PROTEAN® TGX™ precast protein gel (Bio-Rad #4561084) under reducing conditions (dithiothreitol 10 %, Sample Reducing Agent 10 ×, Invitrogen #NP0009) and transferred onto a nitrocellulose membrane (Trans-blot Turbo Transfer pack, 0.2 μm nitrocellulose, Bio-Rad #1704159). Blots were incubated overnight with the primary antibody at 4 °C, and then for 1 h with the appropriate DyLight 680 or 800 Fluor-conjugated secondary antibody (Thermo Fisher Scientific #35568 and #35521). The primary antibodies used were rabbit anti-CYP1A1 (1:1000, Proteintech #3241- 1-AP), mouse anti-vinculin (1:5000, Sigma-Aldrich V9131) and mouse anti-actin (1:5000, Sigma-Aldrich A5441). Secondary antibodies were DyLight 800- labeled anti-mouse (1:20,000, Thermo Fisher Scientific #35521) or DyLight 680-labeled anti-rabbit (1:20,000, Thermo Fisher Scientific #35568). Primary and secondary antibodies were diluted in the following dilution buffer: 1X TBS (Sigma-Aldrich RDD009), 0.1 % Tween-20 (Tween®20 Prolabo™ 28829.183), 5 % nonfat dry milk (Régilait®), 0.1 % sodium azide (Sigma-Aldrich S8032). Blots were scanned with an Odyssey® Imaging System (Li-COR, Bad Homburg, Germany). Quantification was performed using the Li-COR Odyssey software (Version 3.0.25).

2.14. Transmission electron microscopy (TEM)

The CeO_2 NPs were observed by transmission electron microscopy (TEM). CeO_2 NPs were suspended in the placental culture medium at a concentration of 3 mg/mL and sonicated for 2 min as described before. CeO_2 NPs were adsorbed on Carbon/Formvar 200 mesh copper grids and observed with a Jeol 1400 TEM (Jeol, Croissy-sur-Seine, France) operated at 120 keV and equipped with a RIO CMOS camera (Ametek SAS, Elancourt, France).

2.15. Statistical analysis

Statistical tests were performed using the GraphPad Prism 10.0.2 software (La Jolla, CA, USA). The results of the quantitative analyses are presented as mean ± standard error of the mean (SEM). The Shapiro–Wilks normality test was performed to determine whether the samples followed a normal distribution. Differences between groups were evaluated with the parametric one-way ANOVA Dunnett or paired *t*-test for samples with a normal distribution and with a non-parametric test followed by a Wilcoxon post-hoc for samples with a non-normal distribution. A p-value lower than 0.05 was considered to be statistically significant, with $P < 0.05$, $P < 0.01$, $P < 0.001$ and $P < 0.0001$ represented as *, **, *** and ****, respectively.

3. Results

3.1. Characterization of benzo(a)pyrene-coated cerium dioxide nanoparticles

Both uncoated and BaP-coated CeO_2 NPs at high and low ratios were analyzed by TEM (Fig. 1A), while DLS was used to assess the agglomeration/aggregation of BaP-coated CeO_2 NPs at both ratios, as well as CHX-treated CeO_2 NPs (Table 1). No marked difference in shape and size of the particles was observed by TEM after coating with low and high ratio of BaP (Fig. 1A) and particles have the same morphology and are within the size range than indicated by the provider (10 - 100 nm). The size range of these reference particles is in line with airborne cerium oxide which will be heterogeneous in size in the environment. The size of CeO_2 NPs emitted into the air by diesel vehicles using Envirox™ fuel additive is for instance about 50–300 nm. The hydrodynamic diameter of CHX-treated CeO_2, LR and HR BaP-coated CeO_2 NPs was measured after incubation in both placental and bronchial culture media for 0, 24, and 48 h (Table 1). DLS measurements showed agglomeration of CeO_2 NPs with and without coating in both culture media with a hydrodynamic diameter > 200 nm, compared to the diameter of 10 - 100 nm of single particles (Table 1). However, no major difference was observed in each medium between CHX-treated CeO_2 NPs, LR and HR BaP-coated CeO_2 NPs (Figs. 1B, S1). A higher hydrodynamic diameter was observed in bronchial medium (between 450 - 1120 nm) compared to placental medium (between 180 - 370 nm). The differences in composition of each culture medium and their protein content may explain the lower agglomeration in the placental compared to the bronchial medium. These observations show that BaP coating did not modify the agglomeration/aggregation state of CeO_2 NPs in the bronchial and placental exposure media.

To assess the actual concentration of CeO_2 NPs deposited on the cells, the effective density of CeO_2 NPs in bronchial and placental media was calculated using volume centrifugation method (3 g/cm^3) and used, along with DLS data, in the DosiGUI software within the DG model. The DosiGUI simulation confirmed that the totality of the particles (approximately 80 μg/cm^2) deposited on the cells after a short incubation time of 1 hour.

3.2. Assessment of coating stability

The amount of adsorbed BaP on CeO_2 NPs was quantified by HPLC after desorption by incubation in acetonitrile (Table 2). BaP LR and HR coating ratio were 2.08 ± 0.03 and 8.56 ± 0.25 μg (BaP)/mg (CeO_2) respectively. To confirm coating stability after sonication in cell culture medium, free BaP was measured after sonication in bronchial and placental culture media. BaP losses of 15–22 % for the low ratio and 5–12 % for the high ratio were observed (Table 2). The final amount of

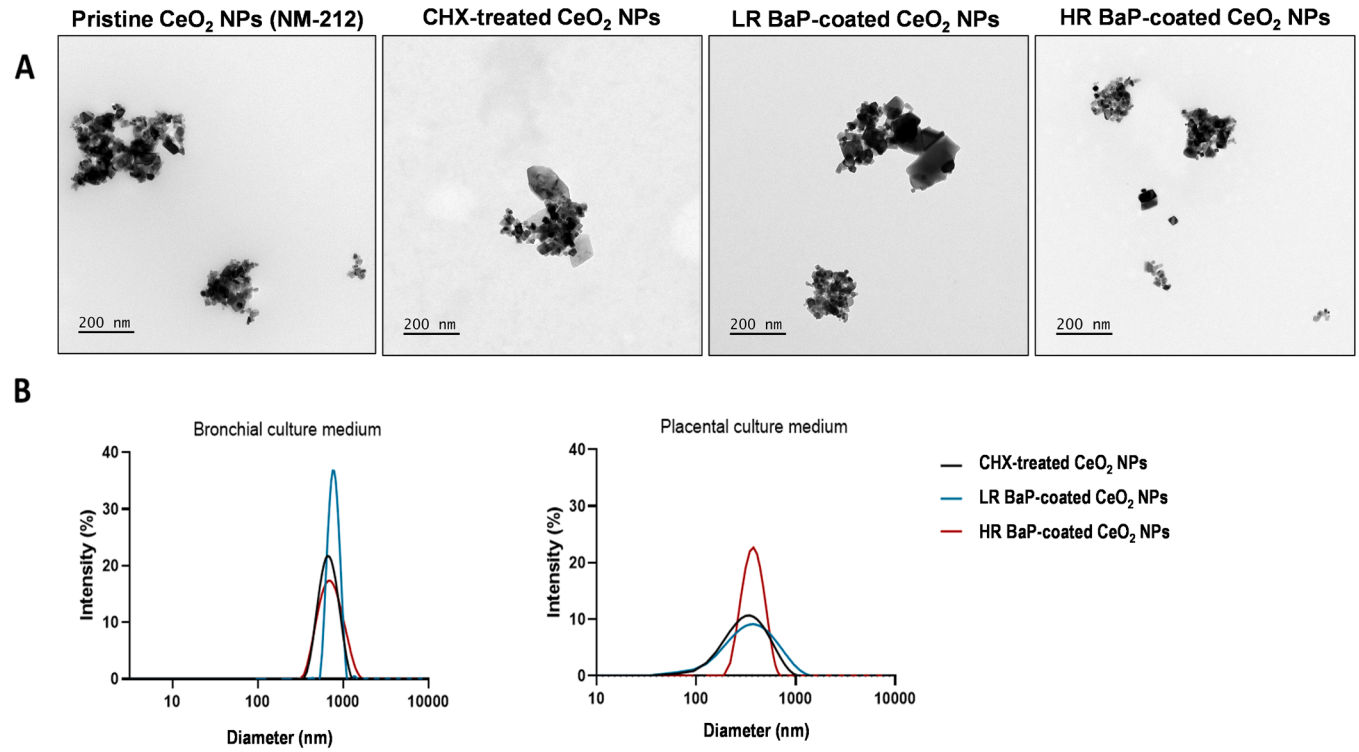

Fig. 1. Characterization of pristine CeO_2 NPs, CHX-treated CeO_2 NPs and BaP-coated CeO_2 NPs at low and high ratios by TEM and DLS. (A) Representative TEM images of pristine CeO_2 NPs (NM-212), CHX-treated CeO_2 NPs and BaP-coated CeO_2 NPs at LR and HR. Scale bar is 200 nm. **(B)** Hydrodynamic diameter of CHX-treated CeO_2 NPs and BaP-coated CeO_2 NPs measured in the bronchial and placental culture medium after 48 h incubation at 37 °C.

Table 1
Hydrodynamic diameter of CHX-treated and BaP-coated CeO_2 NPs measured by DLS in bronchial and placental culture media after 0, 24, 48 h. Mean ± standard deviation of 3 replicates.

Hydrodynamic Diameter (nm)				
Time (h)	Cell Culture Media	CHX-treated CeO_2 NPs	LR BaP-coated CeO_2 NPs	HR BaP-coated CeO_2 NPs
0	Bronchial	448 ± 24	557 ± 78	504 ± 25
	Placental	241 ± 14	183 ± 6	211 ± 6
24	Bronchial	760 ± 67	1126 ± 106	983 ± 71
	Placental	308 ± 59	264 ± 17	372 ± 94
48	Bronchial	651 ± 89	683 ± 150	643 ± 66
	Placental	193 ± 47	268 ± 53	223 ± 139

Table 2
Detection and quantification of BaP adsorption and desorption on CeO_2 NPs by HPLC. BaP was extracted of CeO_2 NPs using acetonitrile. The measured ratio represents µg of BaP per 1 mg of CeO_2 NPs. For the measured ratio, three replicates of each preparation have been done. To detect BaP desorption in culture media, BaP-coated CeO_2 NPs were resuspended in culture media and sonicated. Suspension was centrifuged and the supernatant was diluted in acetonitrile to extract BaP in solution (2 independent measurements). Mean values ± SEM.

Coating ratio	Measured ratio µg (BaP)/ mg (CeO_2 NPs)	Culture Medium	Post-sonication ratio in culture medium µg (BaP) / mg (CeO_2 NPs)	BaP loss (%)
LR	2.08 ± 0.03	Bronchial	1.8 ± 0.2	15.4
		Placental	1.6 ± 0.1	22.5
HR	8.56 ± 0.25	Bronchial	8.1 ± 0.3	5.4
		Placental	7.5 ± 0.4	12.5

adsorbed BaP per mg of CeO_2 NPs was 1.8 ± 0.2 for LR and 8.1 ± 0.3 µg for HR in the bronchial medium; and 1.6 ± 0.1 µg for LR and 7.5 ± 0.4 µg for HR in the placental medium.

The loss of BaP could be due to the sonication at high energy or to loss during preparation for HPLC analysis, thus the stability of BaP coating was further analyzed by ATR-FTIR. The characteristic vibrational modes of BaP in CHX are visible at 885, 850, 840, 825, 760, 745, and 690 cm^{-1} (Fig. 2). After sonication of LR BaP-coated CeO_2 NPs in DMEM, the suspensions were centrifuged and the pellet and supernatant were analyzed by ATR-FTIR. The ATR-FTIR spectra show that BaP is detected in the suspension of BaP-coated CeO_2 NPs before centrifugation (Fig. 2) and in the NP pellet (Figure S2), while no BaP is visible in the supernatant (Fig. 2). The absence of BaP in the ATR-FTIR spectrum of the supernatant confirms the stability of BaP adsorption on CeO_2 NPs after sonication in cell culture medium.

BaP can be efficiently desorbed from CeO_2 NPs by CHX (Figure S2), confirming the reversibility of the adsorption process and validating the ATR-FTIR method to detect desorbed BaP.

3.3. *Cell viability assessment*

We evaluated the biological effects of exposures by assessing their cytotoxicity in NHBE cells and human primary trophoblasts (VCT) using the WST-1 assay which measures the metabolic activity of the cultures (Fig. 3). To this end, both cell types were exposed for 48 h to CeO_2 NPs or BaP alone, co-exposed to free BaP and CeO_2 NPs and exposed to BaP coated on CeO_2 NPs at high ratio (HR; 6.64 mg/g) and low ratio (LR; 1.66 mg/g), across a broad concentration range. The concentrations were adapted to the bronchial and placenta models to reflect exposure scenario of the different organs, while keeping the same BaP/CeO_2 ratios for HR and LR conditions. Specifically, higher concentrations were used in NHBE cells to simulate direct airway exposure, while lower ranges were included in VCT cells to reflect the reduced levels of pollutants expected to reach the placenta via maternal circulation. However, the

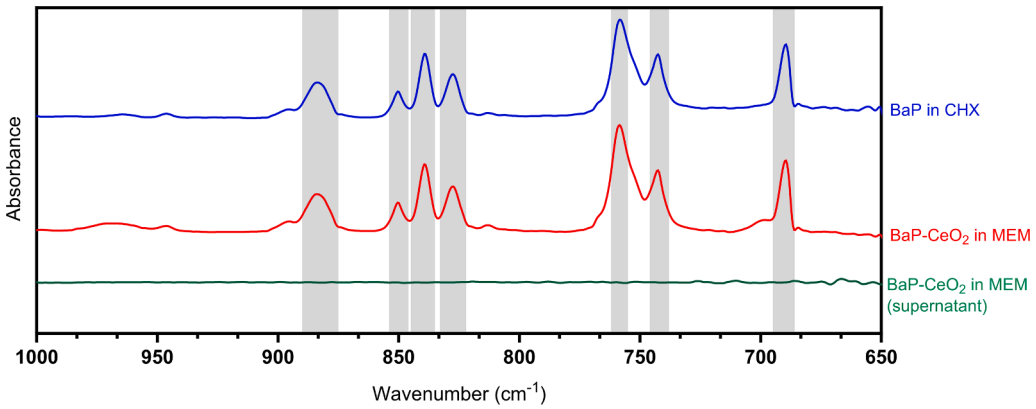

Fig. 2. ATR-FTIR spectra of BaP-coated CeO_2 NPs at low ratio after suspension in culture media. ATR-FTIR spectra of BaP solution in CHX, BaP-coated CeO_2 NPs at low ratio suspended in MEM by sonication, and supernatant after centrifugation.

higher concentrations were also maintained in the placental model to allow for direct comparison between the two cell types under similar exposure conditions.

For the NHBE cells (Fig. 3A), the exposure to CeO_2 NPs alone (at concentrations ranging from 5 to 80 μg/cm^2) induces significant toxicity only at the highest concentration of 80 μg/cm^2 (decreased viability of 22.5 % ± 6.9 compared to control, *$P < 0.05$). Likewise, exposure to BaP alone (at concentrations ranging from 0.5 to 8 μM) show signs of toxicity only at the highest concentration of 8 μM (decreased viability of 15.82 % ± 4.9 compared to control, **$P < 0.01$). For BaP-coated NPs at HR, a significant decrease in viability was already observed from 40 μg/cm^2 of particles, corresponding to 4 μM of BaP if all BaP desorbs from the particle (decreased viability of 12.2 ± 3.9 compared to control, * $P <$ 0.05). However, no significant toxicity was observed for BaP-coated NPs at LR even at the highest concentration of 80 μg/cm^2. When examining co-exposure of CeO_2 NPs and BaP, a significant increase in cytotoxicity was also observed starting from 40 μg/cm^2 of CeO_2 NPs and 4 μM of BaP (decreased viability of 11 % ± 4.9 compared to control, *$P < 0.05$). It is also interesting to note that at the highest concentration of 80 μg/cm^2 of CeO_2 NPs and 8 μM of BaP, the decrease of metabolic activity is significantly higher (75.3 % ± 5.2, #$P < 0.05$) compared to coating at HR at the same concentration (80 μg/cm^2 and 8 μM of BaP if all desorbs from the particles in the experimental setup) (27.3 % ± 4.0). The results suggest synergistic effects between the pollutants in co-exposure compared to single exposures at the same concentrations. We observed similar trends using the Alamar Blue assay which measures the metabolic activity of cultures like WST-1 but with a non-destructive technique (Figure S3 A, $n = 2$).

For the human VCT exposures (Fig. 3B), a broader concentration range was used in order to include the lower pollutant concentrations in maternal blood compared to the concentration of pollutants in the air. Thus, CeO_2 NPs concentrations ranged from 1.25 to 80 μg/cm^2, and BaP concentrations ranged from 0.03 to 8 μM. The exposure to CeO_2 NPs alone induces significant cytotoxicity only at 80 μg/cm^2 (decreased viability of 20.0 % ± 7.7 compared to control, *$P < 0.05$), as observed with the NHBE model. In the placenta model, the highest concentrations of BaP also exhibited cytotoxicity. However, this toxicity is due to cyclohexane solvent rather than BaP itself, as the solvent alone was toxic at the highest concentration: CHX at 2 % (corresponding to the amount of CHX in BaP at 8 μM), decreased metabolic activity by 71.3 % ± 5.7 compared to control (**$P < 0.01$), while the decrease was 62.3 % ± 11.4 for BaP at 8 μM (*$P < 0.05$) and 90.1 % ± 3.9 (**$P < 0.01$) for co-exposure at 8 μM of BaP, both containing CHX at 2 %. Regarding the effect of NPs coated at LR, a significant decrease in cell viability was observed at 80 μg/cm^2 of coated CeO_2 NPs corresponding to 2 μM of BaP if all desorbs (decreased viability of 37.6 % ± 7.6 compared to control, *$P < 0.05$). In contrast, the co-exposure to the free pollutants at 80 μg/cm^2 of particles and 2 μM of BaP, maintained 98.1 % viability at this concentration.

In addition to the results obtained on the metabolic activity of bronchial and placental cells exposed to CeO_2 NPs and BaP, we conducted a second toxicity test by measuring extracellular LDH in the supernatants of cells. The results obtained (Figure S3 B and C) showed only trends without any significant toxicity from the treatments. We performed interference tests with CeO_2 NPs and results show a loss of around 40 % of LDH in presence of CeO_2 NPs in placental medium when measured by Cobas c 701 analyzer with UV test methodology for VCT, and of 15 % when using the Promega kit in the bronchial culture medium for NHBE cells (Table 3). We conclude that the LDH assay cannot be used to assess the cytotoxicity of CeO_2 NPs in our cell models.

3.4. *Impact of pollutants on AhR pathway activation by following CYP1A1 induction*

The impact of co-exposure to BaP and CeO_2 NPs on the AhR detoxifying BaP bioactivation pathway was assessed by comparing the protein levels of CYP1A1 enzyme, a main target gene of this pathway (Fig. 4). We compared the expression of this protein in primary NHBE cells and primary human trophoblasts after 24 h of treatment at non-cytotoxic concentrations as derived from the WST-1 assay. The chosen concentrations were 2 μM BaP and 20 μg/cm^2 CeO_2 NPs for NHBE, 1 μM BaP and 10 μg/cm^2 CeO_2 NPs for VCT.

For NHBE cells, the protein level of CYP1A1 after exposure to 2 μM BaP, while not statistically significant, was 5.9 times higher than the control, ± 1.5. As expected, CeO_2 NPs alone did not activate the AhR pathway, resulting in a CYP1A1 level similar to the control. BaP at 0.5 μM alone or in simultaneous addition with CeO_2 NPs only induced 2.1- and 3.8-fold increases in CYP1A1 expression respectively (Figure S4). For BaP-coated CeO_2 NPs, the coating at LR (corresponding to 0.5 μM of BaP if all desorbs) increased CYP1A1 protein levels by 18.1 times ± 6.0, although this increase was not statistically significant. On the other hand, the coating at HR (corresponding to 2 μM of BaP if all desorbs) significantly increased CYP1A1 protein levels by 35.8 times ± 8.9 compared to the control. As well as for exposure to 2 μM BaP alone, the co-exposure to free BaP at 2 μM and 20 μg/cm^2 CeO_2 NPs did not significantly increase CYP1A1 levels although it was 8.1 fold ± 2.6 compared to the control. Interestingly, a considerable variation in CYP1A1 expression was observed ($P < 0.07$) between HR-coated CeO_2 NPs and both individual BaP exposure and co-exposure to free BaP and CeO_2 NPs at equivalent doses.

For VCT cells, the protein level of CYP1A1 correlates with the amount of BaP used in treatments. At the lower concentration (0.25 μM of BaP), the CYP1A1 protein levels for BaP alone, in co-exposure, and coated on NPs are elevated by 2.7 ± 0.5, 2.9 ± 0.5, and 3.3 ± 0.6,

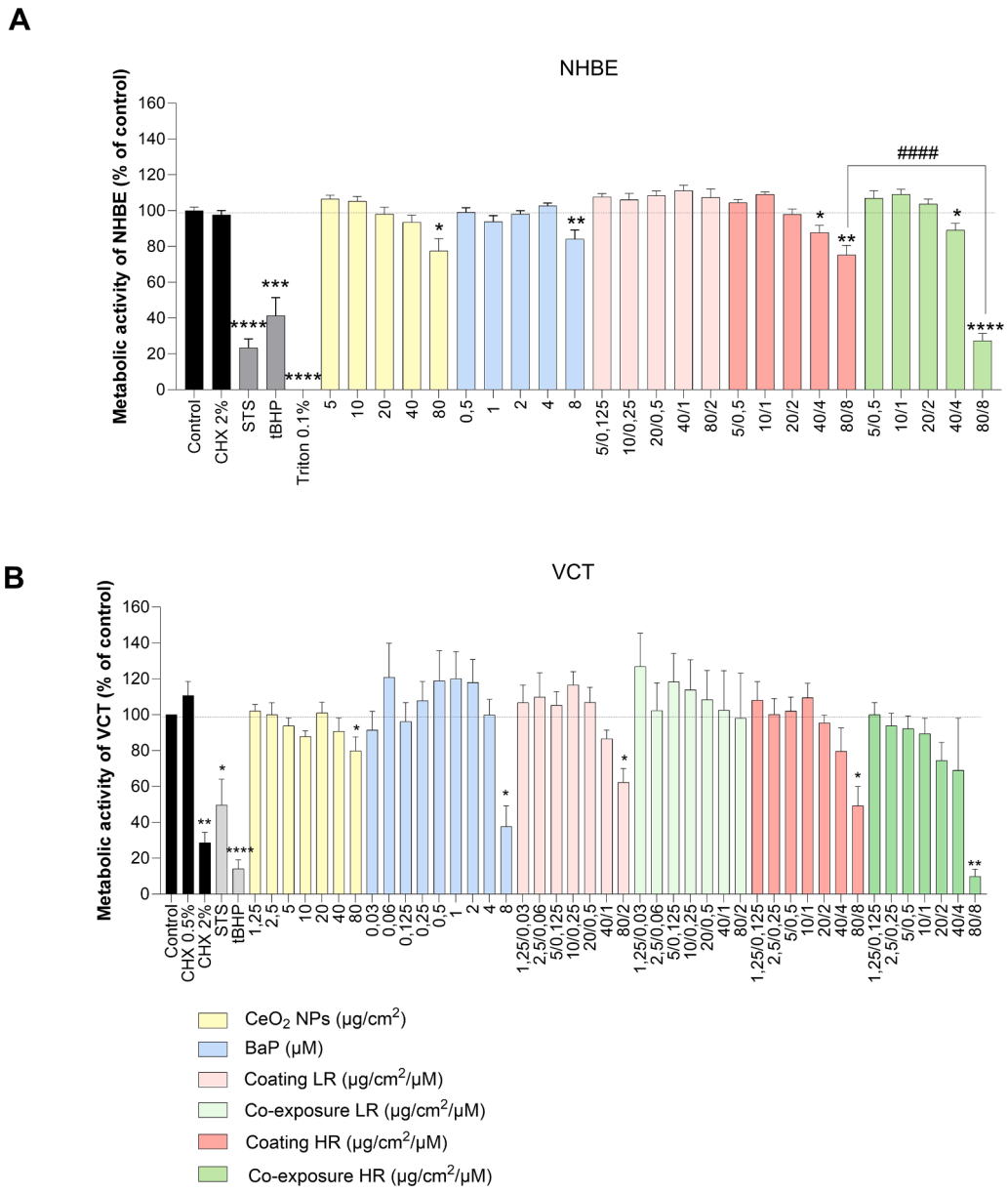

Fig. 3. Cell viability assessment of primary human bronchial epithelial (NHBE) cells and trophoblasts (VTC) exposed to CeO_2 NPs, BaP, and their combinations. Metabolic activity of cultures was evaluated by WST-1 assay after exposure for 48 h to CeO_2 NPs at concentrations ranging from 1.25 to 80 µg/cm^2, BaP at concentrations from 0.03 to 8 µM, co-exposure at a high ratio (co-exposure HR) or low ratio (co-exposure LR) and BaP-coated CeO_2 NPs at both high and low ratios (coating HR and coating LR respectively). Cyclohexane (CHX), Staurosporine (STS), terbutylhydroperoxide (tBHP) and Triton X100 were used as positive controls. **A)** NHBE cell cultures ($n = 3$ independent experiments, with 4 replicates). CHX was used at 2 %, STS at 1.5 µM, tBHP at 500 µM and TritonX100 at 0.1 % for 48h. **(B)** Primary human trophoblasts purified from term placentas ($n = 7$ for CeO_2 NPs and BaP and $n = 3$ for co-exposures and BaP-coated CeO_2 NPs with 3 replicates per placenta), CHX was used at 0.5 and 2 % for 48h, STS at 0.5 µM for 3h and tBHP at 500 µM for 48h. Data are expressed as mean ± SEM. Statistical significance was assessed using a paired *t*-test for normally distributed data and a Wilcoxon test for non-normally distributed data. Significance levels are indicated as follows: $P < 0.05$, $^{**}P < 0.01$, $^{***}P < 0.001$, $^{***}P < 0.0001$ compared to control and #### $P < 0.0001$ compared to co-exposure HR.

Table 3
CeO_2 NPs interference test with LDH assay.

Placental culture medium	LDH (UI/L)	% of LDH compared to control
LDH positive control	1122	100 %
CeO_2 NPs + LDH	670	60 %
Coating HR + LDH	711	63 %
Coating LR +LDH	636	57 %
Bronchial culture medium	**LDH (AU)**	**% of LDH compared to control**
LDH positive control	2026	100 %
CeO_2 NPs + LDH	1719	85 %

respectively, compared to the control. In contrast, at the higher concentration (1 µM of BaP), CYP1A1 protein levels increase to 5.3 ± 0.6, 5.4 ± 0.8, and 4.2 ± 0.5, respectively. Notably, CYP1A1 levels are significantly higher for BaP at 1 µM compared to 0.25 µM (5.3 ± 0.6 versus 2.7 ± 0.5, $P < 0.05$), as well as the coating at HR versus coating at LR (5.4 ± 0.8 versus 2.9 ± 0.5, $\$P < 0.05$).

4. Discussion

With this study, we aimed to enhance the characterization and toxicological evaluation of CeO_2 NPs. Since airborne CeO_2 NPs are often associated with emissions from combustion processes, such as vehicle

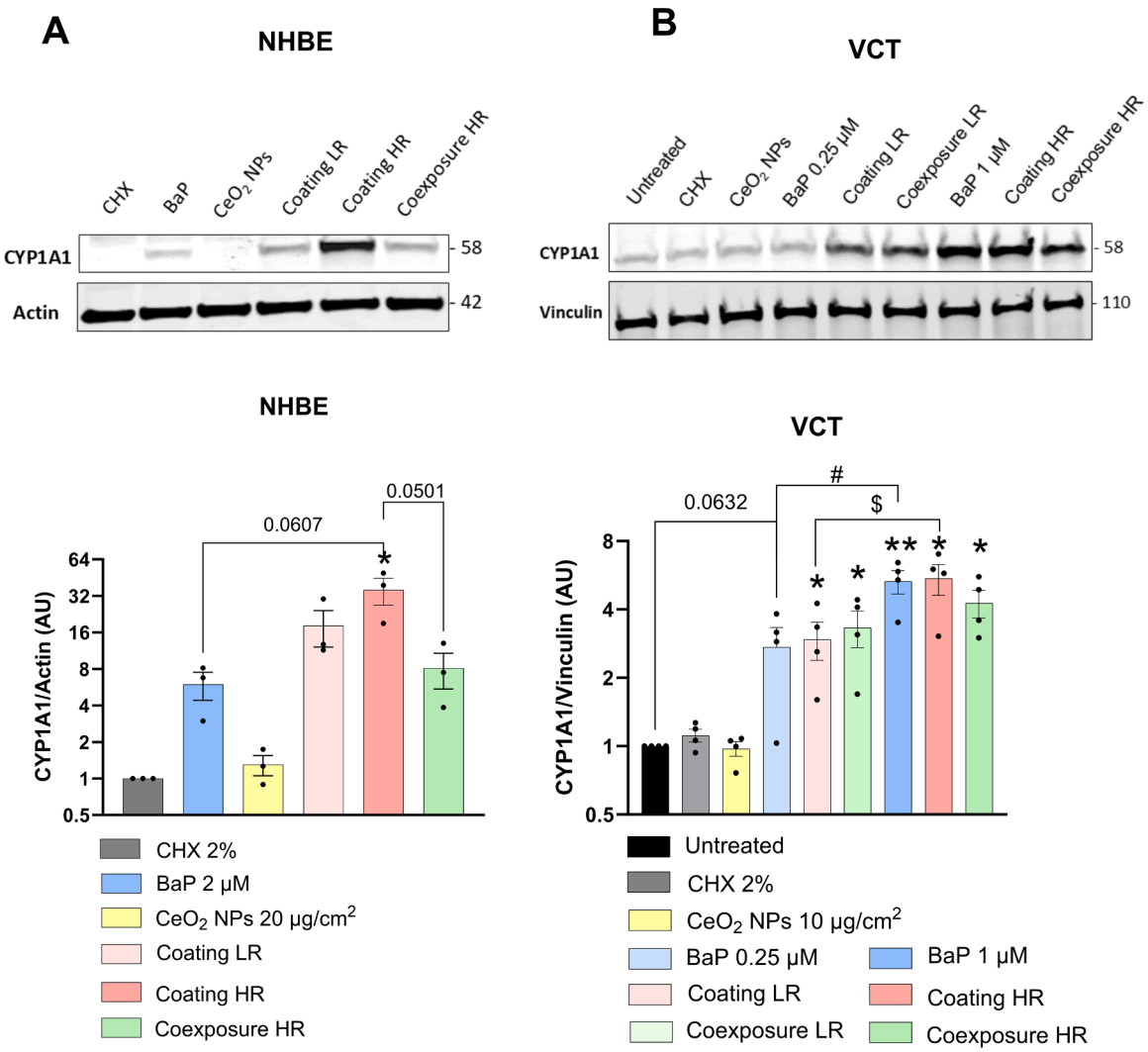

Fig. 4. Effect of BaP and CeO_2 NPs in primary human bronchial epithelial (NHBE) and trophoblasts (VCT) cells on CYP1A1 induction. Western Blot after 24 h of treatment with vehicle control cyclohexane (Ctrl), CeO_2 NPs (CeO_2 NPs), BaP-coated CeO_2 NPs (Coating LR and Coating HR), CeO_2 NPs co-exposed in parallel with free BaP (Co-exposure HR and Co-exposure LR), and BaP alone. Membranes were immunoblotted with anti-CYP1A1, anti-Vinculin antibodies for VCT and anti-Actin for NHBE (loading controls). Immunoblots were quantified with an Odyssey System Imager and the results represent the mean ± SEM after normalization to charging controls ($n = 4$ for VCT and $n = 3$ for NHBE). A representative immunoblot is shown above the respective graphs of NHBE and VCT. Statistical analysis was performed using paired *t*-test; * $P < 0.05$ and ** $P < 0.01$ vs Ctrl, # $P < 0.05$ for BaP LR vs BaP HR, $ $P < 0.05$ for Coating LR vs Coating HR. **(A)** NHBE were treated with particles at 20 µg/cm² and with BaP at 2 µM and cyclohexane at 2 %. **(B)** VCT were treated with particles at 10 µg/cm² , with BaP at 0.25 µM and 1 µM, and with cyclohexane at 0.25 %. Total protein extracts were subjected to SDS-PAGE under reducing conditions.

exhaust from diesel engines (Gantt et al., 2014) equipped with particulate filters (Kumar et al., 2012), cigarette smoke (Böhlandt et al., 2012) and industrial activities (Reed et al., 2014), they can adsorb organic pollutants produced simultaneously by combustion like BaP and other PAH (Szewczyńska et al., 2013; Saenz et al., 2025). Furthermore, given that BaP is recognized as a type 1 CMR (proven Carcinogen, Mutagen, and Reproductive toxicant) as well as an endocrine disruptor (Guarnieri et al., 2023), the study of exposure to this pollutant during pregnancy must be approached with caution. The toxicity of BaP is primarily attributed to its metabolization via the AhR detoxification pathway. Regarding CeO_2 NPs, cytotoxicity and genotoxicity are observed in some cell types, primarily due to mechanisms involving oxidative stress. Their potential toxicity depends on the physicochemical properties of the CeO_2 NPs used (Kang et al., 2023), the type of cells or tissues exposed (Li et al., 2016), the doses, and the duration of exposure. Several studies detecting the presence of cerium in human blood confirm that CeO_2 NPs can cross the pulmonary barrier (Höllriegl et al., 2010). In rats, it is estimated that about 1 % of the inhaled dose in the lungs crosses the pulmonary barrier (Yokel et al., 2014). The study of the impact of CeO_2 NPs on the placental barrier is more recent and requires further investigation. Injection in pregnant mice causes placental dysfunction and adverse pregnancy outcomes (Zhong et al., 2020), and *in vitro* exposure of human trophoblasts to CeO_2 NPs leads to functional disruptions (Nedder et al., 2020).

We had previously characterized and studied the toxicological impact of reference CeO_2 NPs (NM-212 obtained from JRC) alone (Nedder et al., 2020) and in co-exposure with free BaP (Deval et al., 2023) on primary human trophoblasts. These reference CeO_2 NPs (NM-212) are uncoated and free of any capping agent. However, the coating of BaP on NPs more closely reflects environmental exposure scenario than simple co-exposure. Thus, BaP-coated CeO_2 NPs provide an additional tool to better understand the environmental risks to which humans, and particularly pregnant women, may be exposed.

BaP, a planar PAH, can adsorb onto the surface of CeO_2 NPs through various non-covalent interactions, such as Van der Waals, π-π stacking (involving aromatic rings) and hydrophobic interactions. The hydrophobic interactions correspond to the removal of adsorbed water

molecules from the oxide surface, leading to a gain in entropy. Similar adsorption mechanisms have been described for other PAHs on metal oxide surfaces. These interactions are facilitated by physicochemical characteristics of CeO_2 NPs, such as surface oxygen vacancies. In this study, these interactions were taken into account during the preparation of coated NPs by applying solvent evaporation method to adsorb BaP on CeO_2 NPs at two different BaP/ CeO_2 ratios (1.66 mg/g and 6.64 mg/g), controlled drying and resuspension protocols to ensure stable and reproducible surface adsorption.

Our objective was to produce CeO_2 NPs stably coated with BaP at two different ratios to investigate their toxicity on two relevant barrier organ models (bronchial and trophoblastic cells), and the impact of BaP adsorption on CeO_2 NPs on the AhR pathway in comparison to simple co-exposure or exposure to BaP or CeO_2 NPs alone.

For this aim, we chose to use primary cell culture models for both bronchial cells (commercial NHBE) and trophoblastic cells (VCT purified from term human placentas) to study toxicity and activation of the AhR pathway. Unlike cell lines, primary cells have not undergone modifications that increase their resilience to cell death. They maintain xenobiotic metabolizing capacities and retain *in vivo*-like capacities to differentiate and produce hormones (in the case of VCT) or factors (for both VCT and NHBE cells). However, unlike primary bronchial cells, primary trophoblasts do not proliferate *in vitro*. Furthermore, the activation of several signaling pathways may be modified in cell lines. For instance, in the case of BeWo trophoblastic cell lines, the expression and activity of AhR varies depending on the level of confluence in the cultures (Ikuta et al., 2004; Wakx et al., 2018). Moreover, AhR has been reported to be chronically activated in tumors, facilitating tumor progression (Murray et al., 2014). Cell lines derived from cancer cells would therefore not have been the most appropriate model for the study of BaP, one of the AhR ligands. Finally, cell lines lack MRP1 (multidrug resistance-related protein) that contributes to xenobiotic handling (Atkinson et al., 2003).

The first part of this article allowed us to characterize CeO_2 NPs coated with BaP at two different ratios (LR and HR) and demonstrated that this coating did not lead to major differences in the properties of CeO_2 NPs. Indeed, we observed that the agglomeration/aggregation state of these NPs depended primarily on the medium in which they were suspended and showed little variation depending on the BaP coating conditions. This is important to allow comparisons as the agglomeration state will influence the settling *in vitro* as well as the uptake of NPs. The stability of BaP coating on CeO_2 NPs in bronchial and placental culture media was confirmed using HPLC and ATR-FTIR analyses. Thermogravimetric analysis (TGA) and combined TGA-ATR-FTIR could also be considered in future studies to analyze BaP adsorption on different metal oxide NPs.

For toxicity testing, CeO_2 NPs exposure doses were selected based on available data: the lowest concentration (1.25 μg/cm^2) was chosen to align with CeO_2 levels reported in human maternal serum (Heitland and Köster, 2006) or in mouse placenta following intravenous injection (Zhong et al., 2020). BaP levels in the air vary greatly depending on location and season (Bukowska et al., 2022). For dose selection, the lowest BaP concentration (0.03 μM equivalent to 7.68 ng/g dry weight) was chosen to reflect levels detected in human placentas (6.15 ng/g dry weight) (Gladen et al., 2000). The highest concentrations of CeO_2 NPs (80 μg/cm^2) and BaP (8 μM) were used to simulate a potential worst-case exposure scenario. For CYP1A1 induction assays, non-toxic doses were specifically chosen across all exposure conditions, including individual exposure, parallel co-exposure, and BaP-coated CeO_2 NPs, to ensure that observed effects were not confounded by cytotoxicity.

Regarding their potential toxicity on the chosen models, the results of the WST-1 assay showed similar levels of cytotoxicity between primary human bronchial cells and trophoblasts: only the highest concentration at 80 μg/cm^2 of CeO_2 NPs and 8 μM of BaP induced a significant decrease in metabolic activity. However, the toxicity observed at the highest doses in trophoblasts is due to the toxicity of the cyclohexane solvent at these high doses. Therefore, the mechanistic interpretation of BaP-induced effects at 8 μM in VCTs cells is limited, as the observed cytotoxicity may be largely attributed to CHX solvent rather than BaP itself. These high cytotoxic concentrations in trophoblasts are also much higher than the doses of BaP and cerium that can be found in maternal blood (Höllriegl et al., 2010; Wang et al., 2015). We also observed significant cytotoxicity at lower concentrations for co-exposures in bronchial epithelial cells, as well as a notable difference in toxicity between parallel co-exposure and BaP-coated NPs. Indeed, toxicity at comparable ratios is significantly higher during parallel co-exposure compared to coating. This suggests a potential synergistic effect between BaP and CeO_2 NPs when both pollutants are present in their free forms, particularly in NHBE cells.

This tissue-specific difference in toxicity between parallel and coated exposures likely reflects constitutional differences in cell physiology and pollutants handling between bronchial epithelial cells and placental trophoblasts. NHBE are proliferative cells which may render them more sensitive to stress-induced growth arrest or apoptosis. They are also more responsive to AhR ligands such as BaP (6 to 36 times more induction of CYP1A1 in NHBE vs 3 to 5.5 times in VCT as compared to the control) which may enhance cellular response during simultaneous exposure to free BaP and CeO_2 NP, resulting in a synergistic toxic effect. These differences in response depending on the cell type highlight the importance of studying the toxicity of pollutants at all essential barriers for the foetus. It is also possible that BaP adsorbed onto CeO_2 NPs undergoes enhanced metabolization/bioactivation in lung cells compared to free BaP, potentially leading to altered metabolite profiles and detoxification dynamics. This may have important implications in the context of environmental exposure scenarios. In contrast, VCTs are non-proliferative, with intense endocrine activity characterised by high levels of hormone production and secretion, and are generally considered more resistant to apoptosis. The higher toxicity observed with BaP-coated CeO_2 NPs in VCTs may be due to more efficient uptake of the coated particles compared to parallel exposure, potentially facilitated by the semi-barrier property of the placental tissue. This may lead to enhanced intracellular delivery of BaP or different intracellular localization of BaP-coated NPs. In addition, placental cells may differ in their capacity to metabolise and detoxify BaP. Differences in uptake kinetics of NPs, desorption kinetics of BaP from the NP surface or additional BaP-protein interactions that could favour its desorption within the placental microenvironment may also contribute to these effects, particularly as maternal blood is rich in albumin, which is known to bind PAHs like BaP that may influence the release from NP surfaces.

It is important to highlight the potential interferences of NPs with some assays (Ong et al., 2014), as was the case with the LDH assay. Indeed, the interference tests revealed that a significant fraction of LDH could adsorb on CeO_2 NPs, making the results of the cytotoxicity assessment via the LDH assay unreliable.

Then, we demonstrated that the activation levels of the AhR pathway vary depending on both, the cell type and the specific exposure scenario of BaP (alone, parallel co-exposure, and coating). While the level of CYP1A1 induction remained correlated to the quantities of BaP applied to trophoblast cells, primary bronchial epithelial cells induced CYP1A1 in a significantly different manner for the same quantity of BaP added to the cultures, depending on whether cells were exposed to free BaP alone, co-exposed to free BaP and CeO_2 NPs, or exposed to BaP-coated CeO_2 NPs. A non-significant increase in CYP1A1 induction in primary bronchial cells was observed for BaP-coated NPs ($P \sim 0.07$) (but should be interpreted with caution). This may be explained by several hypotheses: a higher internalization of BaP-CeO_2 NPs, a higher bioavailability of BaP, differences in BaP metabolization pathways (leading to different metabolites generated with distinct chemical properties, and/or varying amounts produced) or higher local concentrations of BaP when desorbing from the particles. In contrast, CYP1A1 induction in trophoblasts cells appeared dose-dependent and was less influenced by the mode of exposure, suggesting mechanistic differences in AhR pathway

regulation between the two cell types. These results also suggest that studies of AhR activity should be done systematically when assessing pollutants toxicity in different tissues.

Some studies have already attempted to evaluate the impact of BaP and NPs co-exposure, but they remain scarce and primarily consider only parallel co-exposure without coating. Thus, enhanced effects due to co-exposure have already been observed. For instance, in human umbilical vein endothelial cells (HUVEC), individual BaP and silica NPs exposure did not exhibit cytotoxicity, unlike their co-exposure (Asweto et al., 2017), which induced DNA damage, oxidative stress, cell cycle arrest, and apoptosis. Similarly, co-exposure to silica NPs and BaP, at doses that were non-toxic when applied individually, resulted in pericardial edema and bradycardia in zebrafish embryos, as well as inflammation and erythrocyte aggregation in the caudal vein of these embryos (Duan et al., 2016). The impact of co-exposure to BaP with CeO_2 NPs has been evaluated on gametes (human sperm and rat oocytes). BaP and CeO_2 NPs independently induced DNA damage in gametes, while more pronounced damage was observed following co-exposure in sperm and cumulus cells of rat oocytes (Cotena et al., 2021). CeO_2 NPs coated with BaP, as characterized in this study, provide an additional tool for assessing the impact of organic and inorganic airborne pollutants under conditions that more closely resemble environmental exposure, especially as our results show differences in responses compared to parallel co-exposure in bronchial cells indicating that BaP bioavailability increased when adsorbed on CeO_2 NPs. BaP coating on CeO_2 was stable in culture media suggesting that BaP desorption does take place after interaction with the plasma membranes or internalization of BaP-coated NPs by cells. Intracellular proteins may also act as mediators, where BaP adsorbed on NPs binds first to the protein, desorbing it from the NP, and then to AhR allowing its translocation to the nucleus. The local concentration of BaP at the plasma membrane or inside the cells could thus be increased when coated on CeO_2 NPs. The release and the metabolization pathway of adsorbed PAH following exposure and NP internalization by cells would be an interesting topic of future studies.

5. Conclusion

This study aimed to prepare and characterize BaP-coated CeO_2 NPs and assess their toxicity on bronchial and trophoblastic cells. We confirmed that BaP coating did not significantly alter NP agglomeration but influenced toxicity: bronchial cells showed increased sensitivity in co-exposure compared to BaP-coated NPs. AhR pathway activation varied by cell type, with stronger CYP1A1 induction in bronchial cells for BaP-coated NPs compared to free BaP in single and co-exposure whereas in trophoblasts, CYP1A1 induction remained consistent with the applied BaP concentrations. These results underscore the importance of considering exposure modalities in risk assessment by distinguishing between co-exposure by parallel addition and adsorbed pollutant scenarios, particularly for inhaled pollutants during pregnancy.

CRediT authorship contribution statement

Gaëlle Deval: Writing – review & editing, Writing – original draft, Visualization, Validation, Investigation, Formal analysis, Data curation. **Safaa Mawas:** Writing – review & editing, Writing – original draft, Visualization, Validation, Investigation, Formal analysis, Data curation. **Stéphanie Devineau:** Writing – review & editing, Supervision, Methodology, Formal analysis. **Didier Borderie:** Investigation. **Claire Mikolajczak:** Investigation. **Grégory Lefèvre:** Methodology, Investigation. **Linh-Chi Bui:** Methodology, Investigation. **Justine Renault:** Investigation. **Charlotte Izabelle:** Methodology, Investigation. **Thierry Fournier:** Writing – review & editing. **Ioana Ferecatu:** Writing – review & editing, Supervision, Project administration, Methodology, Funding acquisition. **Sonja Boland:** Writing – review & editing, Supervision, Project administration, Methodology, Funding acquisition, Conceptualization.

Declaration of competing interest

The authors declare that they have no known competing financial interests or personal relationships that could have appeared to influence the work reported in this paper.

Funding

This research was funded by ANR JCJC, a French grant (PregNanoBaP, ANR-20-CE340003) and ANSES funding (BarBaPAhR N° 2015/1/113). G.D. was financed by the French Ministry of Research. This work was funded by the Horizon 2020 Research and Innovation programme (PlasticsFatE project) under the Grant Agreement number 965367. Safaa Mawas was supported by a fellowship from the Ecole Doctorale MTCI, Université Paris Cité. This work was supported by the French National Institute of Health and Medical Research (INSERM) and by Université Paris Cité.

Acknowledgments

The authors would like to express their gratitude to the students who contributed to the development of this project, particularly Laura Segarra, Adrien Mrozik, and Dorian Foissy-Robin, for their assistance. The authors also wish to thank the Cellular and Molecular Imaging Platform (PICMO, UAR612 CNRS, US25 Inserm, Faculté de Pharmacie de Paris, Université Paris Cité, Paris, France), and the Bioprofiler platform of the Unit "Biologie Fonctionnelle et Adaptative", Univ Paris Cité, BFA, UMR 8251 CNRS, F-75205 Paris, France.

Supplementary materials

Supplementary material associated with this article can be found, in the online version, at doi:10.1016/j.hazadv.2025.100802.

Data availability

Data will be made available on request.

References

Arnould, J.P., Verhoest, P., Bach, V., Libert, J.P., Belegaud, J., 1997. Detection of benzo [a]pyrene-DNA adducts in human placenta and umbilical cord blood. Hum. Exp. Toxicol. 16 (12), 716–721. https://doi.org/10.1177/096032719701601204.

Asweto, C.O., Wu, J., Hu, H., Feng, L., Yang, X., Duan, J., Sun, Z., 2017. Combined effect of silica nanoparticles and benzo[a]pyrene on cell cycle arrest induction and apoptosis in Human umbilical vein endothelial cells. Int. J. Env. Res. Public Health 14 (3). https://doi.org/10.3390/ijerph14030289.

Atkinson, D.E., Greenwood, S.L., Sibley, C.P., Glazier, J.D., Fairbairn, L.J., 2003. Role of MDR1 and MRP1 in trophoblast cells, elucidated using retroviral gene transfer. Am. J. Physiol. Cell Physiol. 285 (3), C584–C591. https://doi.org/10.1152/ajpcell.00418.2002.

Böhlandt, A., Schierl, R., Diemer, J., Koch, C., Bolte, G., Kiranoglu, M., Fromme, H., Nowak, D., 2012. High concentrations of cadmium, cerium and lanthanum in indoor air due to environmental tobacco smoke. Sci. Total Env. 414, 738–741. https://doi.org/10.1016/j.scitotenv.2011.11.017.

Bongaerts, E., Nawrot, T.S., Van Pee, T., Ameloot, M., Bové, H., 2020. Translocation of (ultra)fine particles and nanoparticles across the placenta; a systematic review on the evidence of in vitro, ex vivo, and in vivo studies. Part. Fibre Toxicol. 17 (1), 56. https://doi.org/10.1186/s12989-020-00386-8.

Bukowska, B., Mokra, K., Michałowicz, J., 2022. Benzo[a]pyrene-environmental occurrence, Human exposure, and mechanisms of toxicity. Int. J. Mol. Sci. 23 (11). https://doi.org/10.3390/ijms23116348.

Casals, E., Zeng, M., Parra-Robert, M., Fernández-Varo, G., Morales-Ruiz, M., Jiménez, W., Puntes, V., Casals, G., 2020. Cerium oxide nanoparticles: advances in biodistribution, toxicity, and preclinical exploration. Small 16 (20), e1907322. https://doi.org/10.1002/smll.201907322.

Cotena, M., Auffan, M., Tassistro, V., Resseguier, N., Rose, J., Perrin, J., 2021. In vitro Co-exposure to CeO2 nanomaterials from diesel engine exhaust and Benzo(a)Pyrene induces additive DNA damage in sperm and cumulus cells but not in oocytes. Nanomaterials 11 (2), 478. https://doi.org/10.3390/nano10122327.

Dai, M., Huang, W., Huang, X., Ma, C., Wang, R., Tian, P., Chen, W., Zhang, Y., Mi, C., Zhang, H., 2023. BPDE, the migration and invasion of Human trophoblast cells, and occurrence of miscarriage in humans: roles of a novel lncRNA-HZ09. Env. Health Perspect. 131 (1), 17009. https://doi.org/10.1289/ehp10477.

DeLoid, G.M., Cohen, J.M., Pyrgiotakis, G., Pirela, S.V., Pal, A., Liu, J., Srebric, J., Demokritou, P., 2015. Advanced computational modeling for in vitro nanomaterial dosimetry. Part. Fibre Toxicol. 12, 32. https://doi.org/10.1186/s12989-015-0109-1.

Deval, G., Boland, S., Fournier, T., Ferecatu, I., 2021. On placental toxicology studies and cerium dioxide nanoparticles. Int. J. Mol. Sci. 22 (22), 12266. https://doi.org/10.3390/ijms222212266.

Deval, G., Nedder, M., Degrelle, S., Rogozarski, J., Vignaud, M.L., Chissey, A., Colzin, S., Laguillier-Morizot, C., Coumoul, X., Boland, S., Fournier, T., Zerrad-Saadi, A., Ferecatu, I., 2023. Benzo(a)pyrene and cerium dioxide nanoparticles in Co-exposure impair Human trophoblast cell stress signaling. Int. J. Mol. Sci. 24 (6). https://doi.org/10.3390/ijms24065439.

Duan, J., Yu, Y., Li, Y., Wang, Y., Sun, Z., 2016. Inflammatory response and blood hypercoagulable state induced by low level co-exposure with silica nanoparticles and benzo[a]pyrene in zebrafish (Danio rerio) embryos. Chemosphere 151, 152–162. https://doi.org/10.1016/j.chemosphere.2016.02.079.

Duarte-Salles, T., Mendez, M.A., Meltzer, H.M., Alexander, J., Haugen, M., 2013. Dietary benzo(a)pyrene intake during pregnancy and birth weight: associations modified by vitamin C intakes in the Norwegian Mother and Child Cohort Study (MoBa). Env. Int. 60, 217–223. https://doi.org/10.1016/j.envint.2013.08.016.

Gantt, B., Hoque, S., Willis, R.D., Fahey, K.M., Delgado-Saborit, J.M., Harrison, R.M., Erdakos, G.B.., Bhave, P.V., Zhang, K.M., Kovalcik, K., Pye, H.O., 2014. Near-road modeling and measurement of cerium-containing particles generated by nanoparticle diesel fuel additive use. Env. Sci. Technol. 48 (18), 10607–10613. https://doi.org/10.1021/es502169p.

Gladen, B.C., Zadorozhnaja, T.D., Chislovska, N., Hryhorczuk, D.O., Kennicutt 2nd, M.C., Little, R.E., 2000. Polycyclic aromatic hydrocarbons in placenta. Hum. Exp. Toxicol. 19 (11), 597–603. https://doi.org/10.1191/096032700671433928.

Gosens, I., Minnema, J., Boere, A.J.F., Duistermaat, E., Fokkens, P., Vidmar, J., Löschner, K., Bokkers, B., Costa, A.L., Peters, R.J.B, Delmaar, C., Cassee, F.R., 2024. Biodistribution of cerium dioxide and titanium dioxide nanomaterials in rats after single and repeated inhalation exposures. Part. Fibre Toxicol. 21 (1), 33. https://doi.org/10.1186/s12989-024-00588-4.

Guarnieri, G., Becatti, M., Squecco, R., Comeglio, P., Garella, R., Tamburrino, L., Marchiani, S., Vignozzi, L., Vannelli, G.B., Maggi, M., Morelli, A., 2023. Effects of benzo[a]pyrene on the reproductive axis: impairment of kisspeptin signaling in human gonadotropin-releasing hormone primary neurons. Env. Pollut 317, 120766. https://doi.org/10.1016/j.envpol.2022.120766.

Guo, C., Robertson, S., Weber, R.J.M., Buckley, A., Warren, J., Hodgson, A., Rappoport, J.Z., Ignatyev, K., Meldrum, K., Römer, I., Macchiarulo, S., Chipman, J. K., Marczylo, T., Leonard, M.O., Gant, T.W., Viant, M.R., Smith, R., 2019. Pulmonary toxicity of inhaled nano-sized cerium oxide aerosols in Sprague-Dawley rats. Nanotoxicology 13 (6), 733–750. https://doi.org/10.1080/17435390.2018.1554751.

Heitland, P., Köster, H.D., 2006. Biomonitoring of 37 trace elements in blood samples from inhabitants of northern Germany by ICP-MS. J. Trace Elem. Med. Biol. 20 (4), 253–262. https://doi.org/10.1016/j.jtemb.2006.08.001.

Höllriegl, V., González-Estecha, M., Trasobares, E.M., Giussani, A., Oeh, U., Herraiz, M. A., Michalke, B., 2010. Measurement of cerium in human breast milk and blood samples. J. Trace Elem. Med. Biol. 24 (3), 193–199. https://doi.org/10.1016/j.jtemb.2010.03.001.

IARC, 2010. Some non-heterocyclic polycyclic aromatic hydrocarbons and some related exposures. IARC Monogr. Eval. Carcinog. Risks Hum. 92, 1–853.

Ikuta, T., Kobayashi, Y., Kawajiri, K., 2004. Cell density regulates intracellular localization of aryl hydrocarbon receptor. J. Biol. Chem. 279 (18), 19209–19216. https://doi.org/10.1074/jbc.M310492200.

Johnson, N.M., Hoffmann, A.R., Behlen, J.C., Lau, C., Pendleton, D., Harvey, N., Shore, R., Li, Y., Chen, J., Tian, Y., Zhang, R., 2021. Air pollution and children's health-a review of adverse effects associated with prenatal exposure from fine to ultrafine particulate matter. Env. Health Prev. Med. 26 (1), 72. https://doi.org/10.1186/s12199-021-00995-5.

Kang, M.S., Lee, G.H., Kwon, I.H., Yang, M.J., Heo, M.B., Choi, J.W., Lee, T.G., Yoon, C. H., Baek, B., Sung, M.C., Kim, D.W., Park, E.J., 2023. Uptake and toxicity of cerium dioxide nanoparticles with different aspect ratio. Toxicol. Lett. 373, 196–209. https://doi.org/10.1016/j.toxlet.2022.11.013.

Kargozar, S., Baino, F., Hoseini, S.J., Hamzehlou, S., Darroudi, M., Verdi, J., Hasanzadeh, L., Kim, H.W., Mozafari, M., 2018. Biomedical applications of nanoceria: new roles for an old player. Nanomedicine 13 (23), 3051–3069. https://doi.org/10.2217/nnm-2018-0189.

Kliman, H.J., Nestler, J.E., Sermasi, E., Sanger, J.M., Strauss 3rd, J.F., 1986. Purification, characterization, and in vitro differentiation of cytotrophoblasts from human term placentae. Endocrinology 118 (4), 1567–1582. https://doi.org/10.1210/endo-118-4-1567.

Kumar, P.A., Tanwar, M.D., Bensaid, S., Russo, N., Fino, D., 2012. Soot combustion improvement in diesel particulate filters catalyzed with ceria nanofibers. Chem. Eng. J. 207-208, 258–266. https://doi.org/10.1016/j.cej.2012.06.096.

Le Vee, M., Kolasa, E., Jouan, E., Collet, N., Fardel, O., 2014. Differentiation of human placental BeWo cells by the environmental contaminant benzo(a)pyrene. Chem. Biol. Interact. 210, 1–11. https://doi.org/10.1016/j.cbi.2013.12.004.

Leikauf, G.D., Kim, S.H., Jang, A.S., 2020. Mechanisms of ultrafine particle-induced respiratory health effects. Exp. Mol. Med. 52 (3), 329–337. https://doi.org/10.1038/s12276-020-0394-0.

Li, M.D., Chen, L.H., Xiang, H.X., Jiang, Y.L., Lv, B.B., Xu, D.X., Zhao, H., Fu, L., 2024. Benzo[a]pyrene evokes epithelial-mesenchymal transition and pulmonary fibrosis through AhR-mediated Nrf2-p62 signaling. J. Hazard. Mater. 473, 134560. https://doi.org/10.1016/j.jhazmat.2024.134560.

Li, Y., Huang, H., Li, Y., Ye, Z., Li, X., Liu, K., Liu, M., Liu, L., Jiang, J., 2025. Characterizing soil COPs eco-risk in China. J. Hazard. Mater. 489, 137588. https://doi.org/10.1016/j.jhazmat.2025.137588.

Li, Y., Li, P., Yu, H., Bian, Y., 2016. Recent advances (2010-2015) in studies of cerium oxide nanoparticles' health effects. Env. Toxicol. Pharmacol. 44, 25–29. https://doi.org/10.1016/j.etap.2016.04.004.

Mazzolini, J., Weber, R.J., Chen, H.S., Khan, A., Guggenheim, E., Shaw, R.K., Chipman, J.K., Viant, M.R., Rappoport, J.Z., 2016. Protein corona modulates uptake and toxicity of nanoceria via clathrin-mediated endocytosis. Biol. Bull. 231 (1), 40–60. https://doi.org/10.1086/689590.

Miri, A., Akbarpour Birjandi, S., Sarani, M., 2020. Survey of cytotoxic and UV protection effects of biosynthesized cerium oxide nanoparticles. J. Biochem. Mol. Toxicol. 34 (6). https://doi.org/10.1002/jbt.22475 e22475.

Murray, I.A., Patterson, A.D., Perdew, G.H., 2014. Aryl hydrocarbon receptor ligands in cancer: friend and foe. Nat. Rev. Cancer 14 (12), 801–814. https://doi.org/10.1038/nrc3846.

Nedder, M., Boland, S., Devineau, S., Zerrad-Saadi, A., Rogozarski, J., Lai-Kuen, R., Baya, I., Guibourdenche, J., Vibert, F., Chissey, A., Gil, S., Coumoul, X., Fournier, T., Ferecatu, I., 2020. Uptake of cerium dioxide nanoparticles and impact on viability, differentiation and functions of primary trophoblast cells from Human placenta. Nanomaterials 10 (7). https://doi.org/10.3390/nano10071309.

Ong, K.J., MacCormack, T.J., Clark, R.J., Ede, J.D., Ortega, V.A., Felix, L.C., Dang, M.K., Ma, G., Fenniri, H., Veinot, J.G., Goss, G.G., 2014. Widespread nanoparticle-assay interference: implications for nanotoxicity testing. PLoS One 9 (3). https://doi.org/10.1371/journal.pone.0090650 e90650.

Park, B., Donaldson, K., Duffin, R., Tran, L., Kelly, F., Mudway, I., Morin, J.P., Guest, R., Jenkinson, P., Samaras, Z., Giannouli, M., Kouridis, H., Martin, P., 2008. Hazard and risk assessment of a nanoparticulate cerium oxide-based diesel fuel additive - a case study. Inhal. Toxicol. 20 (6), 547–566. https://doi.org/10.1080/08958370801915309.

Paul, E., Franco-Montoya, M.L., Paineau, E., Angeletti, B., Vibhushan, S., Ridoux, A., Tiendrebeogo, A., Salome, M., Hesse, B., Vantelon, D., Rose, J., Canouï-Poitrine, F., Boczkowski, J., Lanone, S., Delacourt, C., Pairon, J.C., 2017. Pulmonary exposure to metallic nanomaterials during pregnancy irreversibly impairs lung development of the offspring. Nanotoxicology 11 (4), 484–495. https://doi.org/10.1080/17435390.2017.1311381.

Reed, K., Cormack, A., Kulkarni, A., Mayton, M., Sayle, D., Klaessig, F., Stadler, B., 2014. Exploring the properties and applications of nanoceria: is there still plenty of room at the bottom? Env. Sci. 46. https://doi.org/10.1039/C4EN00079J.

Saenz, J., Mohammadi, S., Aleman, B., Sapkota, P., Ramirez, K.S., Sharifan, H., 2025. Redox-active cerium dioxide nanoparticles for mitigating anthracene contamination: promising solution to polycyclic aromatic hydrocarbon remediation in stormwater-affected soils. Colloids Surf. A 705, 135657. https://doi.org/10.1016/j.colsurfa.2024.135657.

Saifi, M.A., Seal, S., Godugu, C., 2021. Nanoceria, the versatile nanoparticles: promising biomedical applications. J. Control. Release 338, 164–189. https://doi.org/10.1016/j.jconrel.2021.08.033.

Sheweita, S.A., Al-Shora, S., Hassan, M., 2016. Effects of benzo[a]pyrene as an environmental pollutant and two natural antioxidants on biomarkers of reproductive dysfunction in male rats. Env. Sci. Pollut. Res. Int. 23 (17), 17226–17235. https://doi.org/10.1007/s11356-016-6934-4.

Stone, V., Miller, M.R., Clift, M.J.D., Elder, A., Mills, N.L., Møller, P., Schins, R.P.F., Vogel, U., Kreyling, W.G., Alstrup Jensen, K., Kuhlbusch, T.A.J., Schwarze, P.E., Hoet, P., Pietroiusti, A., De Vizcaya-Ruiz, A., Baeza-Squiban, A., Teixeira, J.P., Tran, C.L., Cassee, F.R., 2017. Nanomaterials versus ambient ultrafine particles: an opportunity to exchange toxicology knowledge. Env. Health Perspect. 125 (10), 106002. https://doi.org/10.1289/ehp424.

Suter, M.A., Aagaard, K.M., Coarfa, C., Robertson, M., Zhou, G., Jackson, B.P., Thompson, D., Putluri, V., Putluri, N., Hagan, J., Wang, L., Jiang, W., Lingappan, K., Moorthy, B., 2019. Association between elevated placental polycyclic aromatic hydrocarbons (PAHs) and PAH-DNA adducts from Superfund sites in Harris County, and increased risk of preterm birth (PTB). Biochem. Biophys. Res. Commun. 516 (2), 344–349. https://doi.org/10.1016/j.bbrc.2019.06.049.

Szewczyńska, M., Pośniak, M., Dobrzyńska, E., Baraniecka, J., 2013. Polycyclic aromatic hydrocarbons distribution in fine and ultrafine particles emitted from diesel engines. Pol. J. Environ. Stud. 22, 553–560.

Val, S., Martinon, L., Cachier, H., Yahyaoui, A., Marfaing, H., Baeza-Squiban, A., 2011. Role of size and composition of traffic and agricultural aerosols in the molecular responses triggered in airway epithelial cells. Inhal. Toxicol. 23 (11), 627–640. https://doi.org/10.3109/08958378.2011.599445.

Wakefield, G., Wu, X., Gardener, M., Park, B., Anderson, S., 2008. Envirox™ fuel-borne catalyst: developing and launching a nano-fuel additive. Technol. Anal. Strateg. Manag. 20 (1), 127–136. https://doi.org/10.1080/09537320701726825.

Wakx, A., Nedder, M., Tomkiewicz-Raulet, C., Dalmasso, J., Chissey, A., Boland, S., Vibert, F., Degrelle, S.A., Fournier, T., Coumoul, X., Gil, S., Ferecatu, I., 2018. Expression, localization, and activity of the aryl hydrocarbon receptor in the Human placenta. Int. J. Mol. Sci. 19 (12). https://doi.org/10.3390/ijms19123762.

Wang, B., Jin, L., Ren, A., Yuan, Y., Liu, J., Li, Z., Zhang, L., Yi, D., Wang, L.L., Zhang, Y., Wang, X., Tao, S., Finnell, R.H., 2015. Levels of polycyclic aromatic hydrocarbons in maternal serum and risk of neural tube defects in offspring. Env. Sci. Technol. 49 (1), 588–596. https://doi.org/10.1021/es503990v.

Wang, R., Wang, W., Ao, L., Wang, Z., Hao, X., Zhang, H., 2017. Benzo[a]pyrene-7,8-diol-9,10-epoxide suppresses the migration and invasion of human extravillous trophoblast HTR-8/SVneo cells by down-regulating MMP2 through inhibition of FAK/SRC/PI3K/AKT pathway. Toxicology 386, 72–83. https://doi.org/10.1016/j.tox.2017.05.008.

Yokel, R.A., Hancock, M.L., Cherian, B., Brooks, A.J., Ensor, M.L., Vekaria, H.J., Sullivan, P.G., Grulke, E.A., 2019. Simulated biological fluid exposure changes nanoceria's surface properties but not its biological response. Eur. J. Pharm. Biopharm. 144, 252–265. https://doi.org/10.1016/j.ejpb.2019.09.023.

Yokel, R.A., Hussain, S., Garantziotis, S., Demokritou, P., Castranova, V., Cassee, F.R., 2014. The Yin: an adverse health perspective of nanoceria: uptake, distribution, accumulation, and mechanisms of its toxicity. Env. Sci. Nano 1 (5), 406–428. https://doi.org/10.1039/c4en00039k.

Zhang, J., Nazarenko, Y., Zhang, L., Calderon, L., Lee, K.B., Garfunkel, E., Schwander, S., Tetley, T.D., Chung, K.F., Porter, A.E., Ryan, M., Kipen, H., Lioy, P.J., Mainelis, G., 2013. Impacts of a nanosized ceria additive on diesel engine emissions of particulate and gaseous pollutants. Env. Sci. Technol. 47 (22), 13077–13085. https://doi.org/10.1021/es402140u.

Zhang, J.J., Lee, K.B., He, L., Seiffert, J., Subramaniam, P., Yang, L., Chen, S., Maguire, P., Mainelis, G., Schwander, S., Tetley, T., Porter, A., Ryan, M., Shaffer, M., Hu, S., Gong, J., Chung, K.F., 2016. Effects of a nanoceria fuel additive on the physicochemical properties of diesel exhaust particles. Env. Sci. Process Impacts 18 (10), 1333–1342. https://doi.org/10.1039/c6em00337k.

Zhang, Z.H., Balasubramanian, R., 2017. Effects of cerium oxide and ferrocene nanoparticles addition As fuel-borne catalysts on diesel engine particulate emissions: environmental and health implications. Env. Sci. Technol. 51 (8), 4248–4258. https://doi.org/10.1021/acs.est.7b00920.

Zhao, Y., Chen, X., Liu, X., Ding, Y., Gao, R., Qiu, Y., Wang, Y., He, J., 2014. Exposure of mice to benzo(a)pyrene impairs endometrial receptivity and reduces the number of implantation sites during early pregnancy. Food Chem. Toxicol. 69, 244–251. https://doi.org/10.1016/j.fct.2014.04.021.

Zhong, H., Geng, Y., Chen, J., Gao, R., Yu, C., Yang, Z., Chen, X., Mu, X., Liu, X., He, J., 2020. Maternal exposure to CeO(2)NPs during early pregnancy impairs pregnancy by inducing placental abnormalities. J. Hazard. Mater. 389, 121830. https://doi.org/10.1016/j.jhazmat.2019.121830.